

MICRO-MECHANICS OF THE MECHANICAL PROPERTIES OF COMPOSITES WITH FRACTAL FIBER LENGTH DISTRIBUTION

WENLONG TIAN^{Ⓜ,*†,||,††} LU ZHU^{Ⓜ,†} XUJIANG CHAO^{Ⓜ,‡} LEHUA QI^{Ⓜ,†,**,††}
and M. W. FU^{Ⓜ,§,¶}

**Research & Development Institute of
Northwestern Polytechnical University in Shenzhen
Shenzhen 518057, P. R. China*

*†School of Mechanical Engineering
Northwestern Polytechnical University
Xi'an 710072, P. R. China*

*‡Institute of Textiles and Clothing
The Hong Kong Polytechnic University
Hong Kong, P. R. China*

*§Department of Mechanical Engineering
The Hong Kong Polytechnic University
Hong Kong, P. R. China*

*¶Research Institute for Advanced Manufacturing
The Hong Kong Polytechnic University
Hong Kong, P. R. China*

||tianwenlong_me@nwpu.edu.cn

***qilehua@nwpu.edu.cn*

††Corresponding authors.

This is an Open Access article in the “Special issue section on Fractals in Advanced Textiles, Intelligent Wearables, and Fashionable Clothing”, edited by Dahua Shou[Ⓜ] (The Hong Kong Polytechnic University, Hong Kong, China), Kausik Bal[Ⓜ] (University of Calcutta, India), Jianlong Kou[Ⓜ] (Zhejiang Normal University, China) & Wan Shou[Ⓜ] (Massachusetts Institute of Technology, USA) published by World Scientific Publishing Company. It is distributed under the terms of the Creative Commons Attribution 4.0 (CC BY) License which permits use, distribution and reproduction in any medium, provided the original work is properly cited.

Received February 4, 2022
 Accepted May 12, 2022
 Published November 28, 2023

Abstract

In short-fiber composites (SFCs), fiber length distribution (FLD) is complicated and has a considerable impact on the mechanical properties of SFCs. This work proposes a fractal FLD in SFCs on the basis of the fractal theory, and develops a multi-step mean-field homogenization (MSMFH) method to accurately and efficiently predict the mechanical properties of SFCs with fractal FLD. In the developed MSMFH method, SFCs are first decomposed into virtual pseudo-grains (PGs) according to fiber orientation distribution (FOD), followed the further division of the PGs into virtual sub-pseudo-grains (SPGs) according to FLD. The Mori–Tanaka or Double-Inclusion model is adopted to homogenize the mechanical properties of each SPG in the first step, and the Voigt model is implemented to homogenize the mechanical properties of all the SPGs and the PGs, respectively, in the sequential steps. Fiber length and orientation averaging algorithms for the developed MSMFH method are detailed. The developed MSMFH method and the proposed fractal FLD are validated to accurately predict the mechanical properties of SFCs by the means of the comparison with the FE method and the available experimental tests.

Keywords: Fiber Orientation; Fractal Length Distribution; Mechanical Properties; Micro-Mechanics; Multi-Step Modeling; Short-Fiber Composites.

NOMENCLATURE

(Nomenclature entries should have the units identified)

d = fiber diameter (μm)
 D = fractal dimension
 E_m = matrix elastic modulus (GPa)
 E_f = fiber elastic modulus (GPa)
 l = fiber length (μm)
 l_e = mesh size of the RVE ω (μm)
 L_{RVE} = length of the RVE ω (μm)
 N_f = total number of the divided facets on the unit orientation sphere
 N_t = total number of fibers in the RVE ω
 $N(\gamma)$ = cumulative number of the fibers with the aspect ratio $\geq \gamma$ in the RVE ω
 S_{eq} = equal area of the facets on the unit orientation sphere
 $x_1x_2x_3$ = global cartesian coordinate system attached the RVE ω
 $x_1^Lx_2^Lx_3^L$ = local cartesian coordinate system attached fibers
 v_1 = fiber volume fraction in two-phase composites

v_m = matrix volume fraction in short-fiber composites (SFCs)
 v_f = fiber volume fraction in SFCs
 v_α = volume fraction of the pseudo-grain (PG) ω_α regarding the RVE ω
 $v_{\alpha,\beta}$ = volume fraction of the sub-pseudo-grain (SPG) $\omega_{\alpha,\beta}$ regarding the PG ω_α
 δ_{ij} = the Kronecker's symbol
 φ = fiber Euler orientation angle ($^\circ$)
 γ = fiber aspect ratio
 γ_1 = lower bound of fiber aspect ratio
 γ_m = upper bound of fiber aspect ratio
 θ = fiber Euler orientation angle ($^\circ$)
 ν_m = matrix Poisson's ratio
 ν_f = fiber Poisson's ratio
 ω = RVE of SFCs
 ω_0 = matrix in the RVE ω
 ω_1 = fibers in the RVE ω
 ω_α = PG in the RVE ω
 $\omega_{\alpha,\beta}$ = SPG in the PG ω_α
 Ω = RVE of two-phase composites
 Ω_0 = matrix in the RVE Ω
 Ω_1 = fibers in the RVE Ω
 $\psi(\mathbf{p})$ = fiber orientation probability density function

$\kappa(\gamma)$ = fiber length probability density function

\mathbf{p} = fiber unit orientation vector

\mathbf{u}_j = unit basis vector of the global coordinate system

\mathbf{u}_i^L = unit basis vector of the local coordinate system

$\boldsymbol{\mu}$ = micro-field in the RVE ω

$\langle \boldsymbol{\mu} \rangle_\omega$ = volume-averaged micro-field of the RVE ω

$\langle \boldsymbol{\mu} \rangle_{\omega_\alpha}$ = volume-averaged micro-field of the PG ω_α

$\langle \boldsymbol{\mu} \rangle_{\omega_\alpha}^L$ = volume-averaged micro-field of the PG ω_α in the local coordinate system

$\langle \boldsymbol{\mu} \rangle_{\omega_{\alpha,\beta}}$ = volume-averaged micro-field of the SPG $\omega_{\alpha,\beta}$

$\langle \boldsymbol{\varepsilon} \rangle_{\Omega_0}$ = volume-averaged strain of the matrix in the RVE Ω

$\langle \boldsymbol{\varepsilon} \rangle_{\Omega_1}$ = volume-averaged strain of the fibers in the RVE Ω

$\langle \bullet \rangle_\kappa$ = length-weighted variable over the PG ω_α

$\langle \bullet \rangle_\psi$ = orientation-weighted variable over the RVE ω

\mathbf{B}^ε = strain concentration tensor

\mathbf{C}_0 = stiffness of matrix in two-phase composites (GPa)

\mathbf{C}_1 = stiffness of fibers in two-phase composites (GPa)

\mathbf{H}^ε = strain concentration tensor of the Eshelbys single inclusion problem

\mathbf{I} = the fourth-order symmetric identity tensor

\mathbf{R} = transformation tensor mapping the global and local coordinate systems

\mathbf{S} = the Eshelby's tensor

$\langle \mathbf{C} \rangle_\omega$ = stiffness of the RVE ω (GPa)

$\langle \mathbf{C} \rangle_{\omega_\alpha}$ = stiffness of the PG ω_α (GPa)

$\langle \mathbf{C} \rangle_{\omega_{\alpha,\beta}}$ = stiffness of the SPG $\omega_{\alpha,\beta}$ (GPa)

$\langle \mathbf{C} \rangle_\Omega$ = stiffness of two-phase composites (GPa)

\mathbb{R} = the Euclidean dimension

automotive, building and construction sectors.¹⁻⁴ The accurate characterization of the mechanical properties of SFCs is thus essentially required, and is beneficial for design of SFCs in turn.

The mechanical properties of SFCs strongly depend on their micro-structures, including fiber length distribution (FLD), fiber orientation distribution (FOD) and interfaces between the constituents (i.e. matrix and fibers), among others,^{5,6} besides fiber volume fraction and the mechanical properties of the constituents. Upon to now, there exist a great number of works concerning the cause and effect between the mechanical properties of SFCs and their micro-structures. Most of them focus on the FOD and interfaces,⁷⁻¹⁰ while less of them focus on the FLD.^{11,12} This work emphasizes on the effect of the FLD on the mechanical properties of SFCs.

Regarding characterization of the mechanical properties of SFCs, the related methods are mainly categorized into two groups: experimental and modeling methods. The main advantage of the experimental methods is to provide the most reliable results, while the limitations are labor, cost, and time inefficient.^{13,14} The modeling methods overcome the limitations of the experimental methods, and are increasingly adopted to predict the mechanical properties of SFCs, as an alternative or at least a complement to the experimental methods. The modeling methods can be further divided into two sub-groups: numerical and analytical methods. The former methods are capable of fully considering complicated micro-structures of SFCs and providing more accurate predictions and detailed micro-fields in SFCs. Because of complicated micro-structures of SFCs, viz. the FOD and FLD, computational costs of the numerical methods, however, become expensive. The latter methods possess acceptable prediction accuracy and good computational efficiency, and are generally not available for SFCs.

In the modeling methods, fibers in SFCs are commonly simplified as the cylinders with identical length and radius, and the Representative Volume Elements (RVEs) with this type of fibers are then generated and used to predict the mechanical properties of SFCs. To predict the elastic properties of SFCs, Mentges *et al.*¹⁵ proposed an artificial neural networks model, in which the training and validating data was generated by developing a two-step micro-mechanical method comprising of the

1. INTRODUCTION

Owing to light-weight, excellent thermo-mechanical properties and economical fabrication processes, short-fiber composites (SFCs) have spread their applications to aerospace, automotive, marine,

orientation averaging method and the finite element homogenization (FEH) method with the RVEs containing identical length and diameter of fibers. Compared with the available experimental results, the proposed artificial neural networks model was validated. Babu *et al.*¹⁶ studied capability of the RVEs containing the fibers with identical length and radius and with different orientations to predict the elastic properties of SFCs. The agreement with the results of the non-RVE methods indicated the effectiveness of the employed RVEs. In Ref. 17, an RVE model with embedded solid elements was developed to homogenize the mechanical properties of SFCs, and the fibers with identical length and radius were included in the RVE model. Through the comparison with the results of the Digimat, the RVE model was verified to yield accurate estimations of the mechanical properties of SFCs. Though the satisfying predictions are obtained, this simplification of fiber length is completely not consistent with that in actual SFCs.

The investigations have indicated that the FLD in SFCs is dominantly determined by fabrication parameters, which contribute to variation of mechanical shearing and inter-fiber friction, and thus fiber breakage. Regarding the SFCs produced by injection molding and extrusion processes, the Weibull FLD is generally hypothesized.^{11,12} The hypothesis, however, is probably inaccurate to describe the FLD in certain SFCs.¹⁸ On the basis of the fractal theory that random objectives often follow the fractal geometry,^{19,20} this work proposes a new fractal FLD in SFCs and develops a multi-step mean-field homogenization method (MSMFH, one of the analytical methods) to achieve the accurate and efficient predictions of the mechanical properties of SFCs with the fractal FLD.

The following structure of the paper is organized. Following this introduction, the mean-field homogenization (MFH) theory and the related MFH models for predicting the mechanical properties of two-phase composites are presented in Sec. 2. In Sec. 3, the MSMFH method to predict the mechanical properties of SFCs is proposed. Sections 4 and 5 present the fractal FLD and the detailed fiber length and orientation averaging algorithms. The developed MSMFH method and the proposed fractal FLD are validated in Sec. 6. Section 7 concludes.

2. MEAN-FIELD HOMOGENIZATION OF TWO-PHASE COMPOSITES

Two-phase composites here consist of matrix, fibers with same size and orientation and perfect interfaces between the constituents. A macroscopical linear displacement boundary condition is imposed on the RVE of the composites, and the volume-averaged strain of the matrix is related to that of the fibers as

$$\langle \boldsymbol{\varepsilon} \rangle_{\Omega_1} = \mathbf{B}^\varepsilon : \langle \boldsymbol{\varepsilon} \rangle_{\Omega_0}. \quad (1)$$

\mathbf{B}^ε differs for various MFH models.²¹ The stiffness of the composites then takes the following expression for any MFH model defined by \mathbf{B}^ε :

$$\langle \mathbf{C} \rangle_{\Omega} = [(1 - v_1)\mathbf{C}_0 + v_1\mathbf{C}_1 : \mathbf{B}^\varepsilon] : [(1 - v_1)\mathbf{I} + v_1\mathbf{B}^\varepsilon]^{-1}, \quad (2)$$

where $\mathbf{I} = (\delta_{ik}\delta_{jl} + \delta_{il}\delta_{jk})/2$.

The Voigt model²² presumes the same uniform strain in the matrix and fibers, i.e. $\langle \boldsymbol{\varepsilon} \rangle_{\Omega_0} = \langle \boldsymbol{\varepsilon} \rangle_{\Omega_1}$, and thus $\mathbf{B}^\varepsilon = \mathbf{I}$. The stiffness of the composites is then derived as

$$\langle \mathbf{C} \rangle_{\Omega} = (1 - v_1)\mathbf{C}_0 + v_1\mathbf{C}_1. \quad (3)$$

By contrast, the same uniform stress in the matrix and fibers are assumed in the Reuss model,²³ i.e. $\langle \boldsymbol{\varepsilon} \rangle_{\Omega_0} = \langle \boldsymbol{\varepsilon} \rangle_{\Omega_1}$, and thus $\mathbf{B}^\varepsilon = \mathbf{C}_0 : \mathbf{C}_1^{-1}$. The stiffness of the composites is then computed by the following equation:

$$\langle \mathbf{C} \rangle_{\Omega} = [(1 - v_1)\mathbf{C}_0^{-1} + v_1\mathbf{C}_1^{-1}]^{-1}. \quad (4)$$

The Voigt and Reuss models theoretically provide the upper and lower bounds of the stiffness of the composites, respectively.

In addition to the Voigt and Reuss models, the Mori-Tanaka (MT) model²⁴ and Double-Inclusion (DI) model²⁵ are the commonly used MFH models and are derived based on the fundamental solution of the Eshelby's single inclusion problem,²⁶ in which the strain concentration tensor is expressed as

$$\mathbf{H}^\varepsilon(\mathbf{C}_0, \mathbf{C}_1) = \{\mathbf{I} + \mathbf{S} : [\mathbf{C}_0^{-1} : \mathbf{C}_1 - \mathbf{I}]\}^{-1}. \quad (5)$$

\mathbf{S} is determined by the matrix Poisson's ratio and fiber aspect ratio.

Regarding the MT model, the strain concentration tensor is identical with that of the Eshelby's

single inclusion problem, which implies

$$\mathbf{B}^\varepsilon = \mathbf{H}^\varepsilon(\mathbf{C}_0, \mathbf{C}_1). \quad (6)$$

The stiffness of the composites is thus determined by substituting Eq. (6) to Eq. (2).

For the DI model, the following interpolative strain concentration tensor²⁷ is generally adopted:

$$\mathbf{B}^\varepsilon = \{[1 - \xi(v_1)](\mathbf{B}_{\text{lower}}^\varepsilon)^{-1} + \xi(v_1)(\mathbf{B}_{\text{upper}}^\varepsilon)^{-1}\}^{-1}, \quad (7)$$

where $\mathbf{B}_{\text{lower}}^\varepsilon$ is the strain concentration tensor of the MT model and $\mathbf{B}_{\text{upper}}^\varepsilon$ is the strain concentration tensor of the reverse MT model²⁷:

$$\begin{aligned} \mathbf{B}_{\text{lower}}^\varepsilon &= \mathbf{H}^\varepsilon(\mathbf{C}_0, \mathbf{C}_1) \quad \text{and} \\ \mathbf{B}_{\text{upper}}^\varepsilon &= [\mathbf{H}^\varepsilon(\mathbf{C}_1, \mathbf{C}_0)]^{-1}. \end{aligned} \quad (8)$$

The smooth interpolation function $\xi(v_1)$ takes the quadratic expression of v_1 :

$$\xi(v_1) = \frac{1}{2}v_1(1 + v_1). \quad (9)$$

Substituting Eqs. (7)–(9) to Eq. (2), the stiffness of the composites is finally computed.

3. MULTI-STEP MEAN-FIELD HOMOGENIZATION OF SHORT-FIBER COMPOSITES

Here SFCs consist of matrix, a great number of short (cylindrical) fibers and perfect interfaces between them. Material properties and diameters of the fibers are identical, while lengths and orientations of the fibers are different. Consider an RVE of the SFCs, in which each fiber i is uniquely characterized by its own aspect ratio γ (i.e. l/d) and

unit orientation vector \mathbf{p} . In the global (cartesian) coordinate system attached the RVE, \mathbf{p} is defined by the Euler orientation angles: $\theta \in [0, \pi]$ between \mathbf{p} and the axis x_1 and $\phi \in [0, 2\pi]$ between the projection of \mathbf{p} on the plane x_2ox_3 and the axis x_1 , as illustrated in Fig. 1:

$$\mathbf{p} = [\sin \theta \cos \varphi, \sin \theta \sin \varphi, \cos \theta]^T. \quad (10)$$

The FLD and FOD in the RVE, on the other hand, are characterized by the fiber length and orientation distribution functions, respectively, which express that the probability of the fibers with the aspect ratios between γ and $\gamma + d\gamma$ is $\kappa(\gamma)d\gamma$, and the probability of the fibers with the orientations between \mathbf{p} and $\mathbf{p} + d\mathbf{p}$ is $\psi(\mathbf{p})d\mathbf{p}$, respectively.

The fibers in the RVE are first grouped into N sets based on their orientations, each of which has a volume fraction of $v_{f,\alpha}$ regarding the RVE:

$$v_m + \sum_{\alpha=1}^N v_{f,\alpha} = 1. \quad (11)$$

For each set (α), the orientations of the fibers are between \mathbf{p}_α and $\mathbf{p}_\alpha + d\mathbf{p}$ and the FLD is identical with that of the RVE. The matrix of the RVE is accordingly grouped into N sets such that the volume fraction $v_{m,\alpha}$ of each set regarding the RVE satisfies

$$\sum_{\alpha=1}^N v_{m,\alpha} = v_m \quad \text{and} \quad \frac{v_{f,\alpha}}{v_{m,\alpha} + v_{f,\alpha}} = v_f. \quad (12)$$

By combining the matrix set- α and the corresponding fiber set- α , N pseudo-grains (PGs), which assemble the RVE, are generated, and each PG is

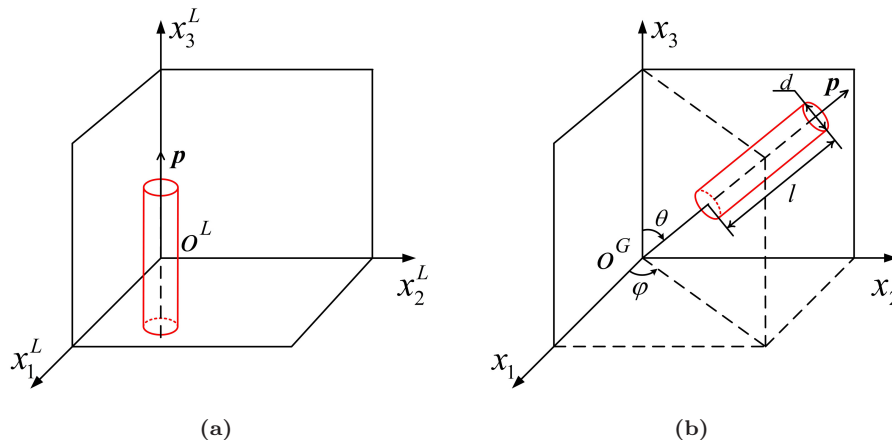


Fig. 1 An oriented fiber in the (a) local coordinate system $x_1^L x_2^L x_3^L$ and (b) global coordinate system $x_1 x_2 x_3$.

considered as a composite reinforced by the oriented fibers with different lengths. The fiber volume fraction of the PG ω_α is identical with that of the RVE, viz. v_f , and the volume fraction of the PG ω_α regarding the RVE (i.e. all the PGs) is $v_\alpha = v_{f,\alpha}/(1 - v_m) = \psi(\mathbf{p}_\alpha)d\mathbf{p}$.

Regarding the length, the fibers in the PG ω_α are further divided into M sets, each of which has a volume fraction of $v_{f,\beta}$ regarding the PG:

$$v_m + \sum_{\beta=1}^M v_{f,\beta} = 1. \quad (13)$$

The orientations of the fibers are between \mathbf{p}_α and $\mathbf{p}_\alpha + d\mathbf{p}$ and the lengths of the fibers are between γ_β and $\gamma_\beta + d\gamma$ in the set β . Analogically, the matrix in the PG ω_α is divided into M sets, the volume fraction $v_{m,\beta}$ of each of which regarding the RVE satisfies

$$\sum_{\beta=1}^M v_{m,\beta} = v_m \quad \text{and} \quad \frac{v_{f,\beta}}{v_{m,\beta} + v_{f,\beta}} = v_f. \quad (14)$$

The combination of the fiber set- β and the matrix set- β generates M sub-pseudo-grains (SPGs), which assemble the PG ω_α , and each SPG is considered as a two-phase composite containing the oriented fibers with identical length. The fiber volume fraction of the SPG $\omega_{\alpha,\beta}$ is v_f as well, and the volume fraction of the SPG $\omega_{\alpha,\beta}$ regarding the PG ω_α is $v_{\alpha,\beta} = v_{f,\beta}/(1 - v_m) = \kappa(\gamma_\beta)d\gamma$.

For any micro-field (e.g. micro-stress and -strain), its volume average over the RVE is thus expressed by the orientation average of those of the divided PGs^{28,29}:

$$\langle \boldsymbol{\mu} \rangle_\omega = \sum_{\alpha=1}^N \frac{v_\alpha}{(1 - v_m)} \langle \boldsymbol{\mu} \rangle_{\omega_\alpha} = \langle \langle \boldsymbol{\mu} \rangle_{\omega_\alpha} \rangle_\psi, \quad (15)$$

where $\langle \bullet \rangle_\psi$ is defined as follows:

$$\langle \bullet \rangle_\psi = \oint [\bullet \times \psi(\mathbf{p})] d\mathbf{p}. \quad (16)$$

Similarly, the volume-averaged micro-field in the PG ω_α is expressed by the length average of those of the divided SPGs:

$$\langle \boldsymbol{\mu} \rangle_{\omega_\alpha} = \sum_{\beta=1}^M \frac{v_\beta}{(1 - v_m)} \langle \boldsymbol{\mu} \rangle_{\omega_{\alpha,\beta}} = \langle \langle \boldsymbol{\mu} \rangle_{\omega_{\alpha,\beta}} \rangle_\kappa, \quad (17)$$

where $\langle \bullet \rangle_\kappa$ reads as

$$\langle \bullet \rangle_\kappa = \oint [\bullet \times \kappa(\gamma)] d\gamma. \quad (18)$$

Combining Eqs. (15) and (17), the volume-averaged micro-field of the RVE is formulated as

$$\langle \boldsymbol{\mu} \rangle_\omega = \langle \langle \langle \boldsymbol{\mu} \rangle_{\omega_{\alpha,\beta}} \rangle_\kappa \rangle_\psi. \quad (19)$$

Equation (19) indicates that the homogenization of the micro-fields in the RVE can be sequentially conducted through the multi-step method:

- (1) Homogenizing each SPG individually;
- (2) Homogenizing each PG based on the FLD and the homogenized SPGs;
- (3) Homogenizing the RVE based on the FOD and the homogenized PGs.

Therefore, the MSMFH procedure (as shown in Fig. 2): the MT or DI model for each SPG in step (1) homogenization, and the Voigt model for each PG and the RVE in steps (2) and (3) homogenization²⁹ is developed to predict the mechanical properties of the SFCs. Therefore, the stiffness of the SFCs is computed as

$$\langle \mathbf{C} \rangle_\omega = \langle \langle \mathbf{C} \rangle_{\omega_\alpha} \rangle_\psi \quad \text{with} \quad \langle \mathbf{C} \rangle_{\omega_\alpha} = \langle \langle \mathbf{C} \rangle_{\omega_{\alpha,\beta}} \rangle_\kappa. \quad (20)$$

4. FIBER LENGTH AVERAGING METHOD

Fiber lengths are generally simplified to be identical in the numerical/analytical methods to predict the mechanical properties of SFCs, which is, however, not the case in actual SFCs. In this work, the FLD in SFCs is assumed to be fractal. Note that the fiber length is characterized using the fiber aspect ratio due to the identical diameter.

The aspect ratios of the fibers in SFCs are described using an order statistic, which reads as

$$[\gamma_1, \gamma_2, \dots, \gamma_i, \gamma_{i+1}, \dots, \gamma_{m-1}, \gamma_m] \quad \text{with} \quad \gamma_i < \gamma_{i+1}. \quad (21)$$

The cumulative number of the fibers with the aspect ratio $\geq \gamma_i$ and the total number of the fibers in SFCs is computed based on the fractal scaling law,³⁰ respectively:

$$N(\gamma_i) = \left(\frac{\gamma_m}{\gamma_i} \right)^D \quad \text{and} \quad (22)$$

$$N_t = N(\gamma_1) = \left(\frac{\gamma_m}{\gamma_1} \right)^D.$$

Consequently, the probability density function of γ (also known as the length distribution function) is

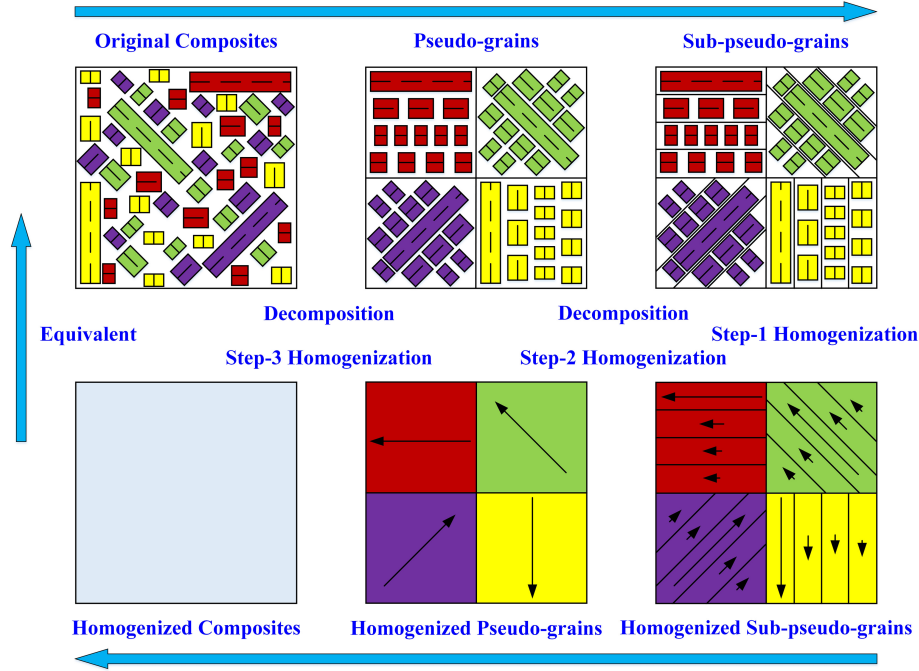


Fig. 2 MSMFH method to predict the mechanical properties of SFCs with different FODs and FLDs.

derived as

$$\kappa(\gamma) = \frac{-dN(\gamma)/d\gamma}{N_t} = D \cdot \gamma_1^D \cdot \gamma^{-(D+1)}. \quad (23)$$

The cumulative probability function of γ is then computed by integrating $\kappa(\gamma)$ within the range of $[\gamma_1, \gamma]$:

$$K(\gamma) = \int_{\gamma_1}^{\gamma} \kappa(\gamma) d\gamma = 1 - \left(\frac{\gamma_1}{\gamma}\right)^D. \quad (24)$$

In the case of $\gamma \rightarrow \gamma_1$, $K(\gamma) \rightarrow 0$, while in the case of $\gamma \rightarrow \infty$, $K(\gamma) \rightarrow 1$. However, γ varies in the range of $[\gamma_1, \gamma_m]$ and $\gamma \rightarrow \gamma_m$ generally does not result to $K(\gamma) \rightarrow 1$. The modified cumulative probability function of γ is thus proposed:

$$K(\gamma) = \left[1 - \left(\frac{\gamma_1}{\gamma}\right)^D\right] \left(\frac{\gamma_m^D}{\gamma_m^D - \gamma_1^D}\right). \quad (25)$$

The fractal dimension of SFCs is related to the fiber volume fraction of SFCs as follows²⁰:

$$D = \mathbb{R} - \frac{\ln(v_f)}{\ln\left(\frac{\gamma_1}{\gamma_m}\right)}, \quad (26)$$

where \mathbb{R} equals 2.0 and 3.0 for the 2D and 3D cases, respectively. Then, we have the following:

$$v_f = \left(\frac{\gamma_1}{\gamma_m}\right)^{\mathbb{R}-D}. \quad (27)$$

The length average integral (i.e. Eq. (18)) for the volume-averaged micro-field of the PG ω_α is discretized as

$$\begin{aligned} \langle\langle \boldsymbol{\mu} \rangle_{\omega_{\alpha,\beta}} \rangle_{\kappa} &= \oint \langle \boldsymbol{\mu}(\gamma) \rangle_{\omega_{\alpha,\beta}} \kappa(\gamma) d\gamma \\ &\approx \sum_{\beta=1}^M \langle \boldsymbol{\mu}(\gamma) \rangle_{\omega_{\alpha,\beta}} \\ &\quad \times \left[\left(\frac{\gamma_1}{\gamma_\beta}\right)^D - \left(\frac{\gamma_1}{\gamma_\beta + \Delta\gamma}\right)^D \right], \end{aligned} \quad (28)$$

where the increment of γ is $\Delta\gamma = \frac{\gamma_m - \gamma_1}{M-1}$ and $\gamma_\beta = \gamma_1 + (\beta-1)\Delta\gamma$. Note that $\Delta\gamma$ is selected to be 0.1 in this work.

5. FIBER ORIENTATION AVERAGING METHOD

5.1. Fiber Orientation Transformation

Fiber orientations of the PGs are different and the mechanical properties of the PGs in the global coordinate system are thus different. To compute the volume-averaged micro-field of SFCs, the volume-averaged micro-fields of the PGs in the local coordinate systems, i.e. the coordinate systems attached to the principal axes of fibers, are required to be

transformed to those in the global coordinate system. This section presents the fiber orientation transformation method relating the global and local volume-averaged micro-fields in the PGs.

The relation between the unit basis vectors of the global and local coordinate systems is given as³¹

$$\mathbf{u}_j = \mathbf{R} \cdot \mathbf{u}_i^L, \quad (29)$$

where \mathbf{R} takes the forms of θ and φ :

$$\mathbf{R} = \begin{bmatrix} \cos \theta \cos \varphi & \cos \theta \sin \varphi & -\sin \theta \\ -\sin \varphi & \cos \varphi & 0 \\ \sin \theta \cos \varphi & \sin \theta \sin \varphi & \cos \theta \end{bmatrix}. \quad (30)$$

The volume-averaged micro-field of the PG ω_α with θ and φ in the global coordinate system is then related to that in the local coordinate system through the following transformation equation:

- For the second-order volume-averaged micro-field $\langle \boldsymbol{\mu}(\theta, \varphi) \rangle_{\omega_\alpha}$ ³²:

$$\langle \boldsymbol{\mu}(\theta, \varphi) \rangle_{\omega_\alpha} = \mathbf{R}^T \cdot \langle \boldsymbol{\mu} \rangle_{\omega_\alpha}^L \cdot \mathbf{R}. \quad (31)$$

- For the fourth-order volume-averaged micro-field $\langle \boldsymbol{\mu}(\theta, \varphi) \rangle_{\omega_\alpha}$ ²⁸:

$$\langle \boldsymbol{\mu}(\theta, \varphi) \rangle_{\omega_\alpha} = \mathbf{R}^T \cdot \mathbf{R}^T \cdot \langle \boldsymbol{\mu} \rangle_{\omega_\alpha}^L \cdot \mathbf{R} \cdot \mathbf{R}. \quad (32)$$

5.2. Fiber Orientation Discretization

This section presents the discretization method of the orientation average integral for calculating the volume-averaged micro-fields of SFCs.³³ The possible orientation vectors of the fibers in SFCs assemble a unit (orientation) sphere, which is then divided into a large number of facets with almost equal areas. The orientation average integral (Eq. (16)) for the volume-averaged micro-field of the RVE is computed by the following equation for the case of 3D fiber orientation:

$$\begin{aligned} \langle \langle \boldsymbol{\mu} \rangle_{\omega_\alpha} \rangle_\psi &= \oint \langle \boldsymbol{\mu}(\mathbf{p}) \rangle_{\omega_\alpha} \psi(\mathbf{p}) d\mathbf{p} \\ &= \int_{\theta=0}^{\pi} \int_{\varphi=0}^{2\pi} \langle \boldsymbol{\mu}(\theta, \varphi) \rangle_{\omega_\alpha} \psi(\theta, \varphi) \sin \theta d\theta d\varphi \\ &\approx 2 \sum_{\alpha=1}^{N_f} \langle \boldsymbol{\mu}(\theta_\alpha, \varphi_\alpha) \rangle_{\omega_\alpha} \psi(\theta_\alpha, \varphi_\alpha) \\ &\quad \times S_{\text{eq}}(\theta_\alpha, \varphi_\alpha) \quad \text{with } \theta_\alpha \in [0, \pi] \\ &\quad \text{and } \varphi_\alpha \in [0, \pi]. \end{aligned} \quad (33)$$

The areas of the divided facets are computed as follows:

- (1) The equal-sized increment of θ is selected to be $\Delta\theta = 1.0^\circ$.
- (2) For the spherical ring situated between the angles $\theta - \Delta\theta/2$ and $\theta + \Delta\theta/2$, its area is calculated as

$$S_\theta = \pi \int_{\theta-\Delta\theta/2}^{\theta+\Delta\theta/2} \sin \tau d\tau = 2\pi \sin \theta \sin \frac{\Delta\theta}{2}. \quad (34)$$

- (3) For the spherical ring $\theta = \pi/2$, the increment of φ is selected as $\Delta\varphi = \Delta\theta$, and the number $N_{\theta=\pi/2}$ and the areas of the equal-size facets on the ring are computed as

$$\begin{aligned} N_{\theta=\pi/2} &= \frac{\pi}{\Delta\varphi} = \frac{\pi}{\Delta\theta} \quad \text{and} \\ S_{\text{eq}} &= \frac{S_{\theta=\pi/2}}{N_{\theta=\pi/2}} = 2\Delta\theta \sin \frac{\Delta\theta}{2}. \end{aligned} \quad (35)$$

- (4) The number N_θ of the equal-size facets in the ring θ and the resulting $\Delta\varphi$ are determined as

$$N_\theta = \frac{S_\theta}{S_{\text{eq}}} = \frac{\pi \sin \theta}{\Delta\theta} \quad \text{and} \quad \Delta\varphi = \frac{\pi}{N_\theta} = \frac{\Delta\theta}{\sin \theta}. \quad (36)$$

- (5) There is just a single facet at the poles $\theta = 0$ and $\theta = \pi$, respectively, and the areas of the facets are derived as

$$S_{\text{eq}} = \pi \int_0^{\Delta\theta/2} \sin \tau d\tau = \pi \left[1 - \cos \frac{\Delta\theta}{2} \right]. \quad (37)$$

Regarding the case of the 2D fiber orientation ($\theta = \pi/2$), the orientation average integral (Eq. (16)) for the volume-averaged micro-field of the RVE is discretized as³³

$$\begin{aligned} \langle \langle \boldsymbol{\mu} \rangle_{\omega_\alpha} \rangle_\psi &= \oint \langle \boldsymbol{\mu}(\mathbf{p}) \rangle_{\omega_\alpha} \psi(\mathbf{p}) d\mathbf{p} \\ &= \int_{\varphi=0}^{2\pi} \langle \boldsymbol{\mu}(\varphi) \rangle_{\omega_\alpha} \psi(\varphi) d\varphi \\ &\approx 2\Delta\varphi \sum_{\alpha=1}^{N_f} \langle \boldsymbol{\mu}(\varphi_\alpha) \rangle_{\omega_\alpha} \\ &\quad \times \psi(\varphi_\alpha) \quad \text{with } \varphi_\alpha \in [0, \pi], \end{aligned} \quad (38)$$

where $N_f = \pi/\Delta\varphi$ and the increment $\Delta\varphi$ of φ is chosen to be $\Delta\varphi = 0.1^\circ$ in this work.

6. VALIDATION OF THE DEVELOPED METHOD

The predicted elastic properties of SFCs with the different FODs and fractal FLDs using the developed MSMFH method are compared to the predictions of the FEH method^{34,35} and the results of the available experimental tests to validate the effectiveness of the developed MSMFH method and the proposed fractal FLD in this section.

In the FEH method, the RVEs of SFCs with the minimum separation distance of $0.05d$ between any two fibers for avoiding distorted meshes are used,^{36,37} and the embedded element technique¹⁷ is introduced to the RVEs for rapidly and conveniently imposing the periodic boundary condition.³⁸ The perfect interfaces between the constituents are hypothesized. The 4-node linear tetrahedron elements are used for meshing the RVEs, and the mesh size l_e is selected such that $L_{RVE}/l_e = 60.0$ to guarantee the converged predictions.

First, the SiC fibers-reinforced 2080 aluminum alloy SFCs,³⁹ in which the fiber volume fractions are 10.0%, 20.0% and 30.0%, respectively, are studied. The linear elastic properties of the matrix and fibers are given as $E_0 = 74.0$ GPa, $\nu_0 = 0.33$ and $E_1 = 410.0$ GPa, $\nu_1 = 0.19$. The second-order orientation vector of the fibers in the SFCs is $\mathbf{a} = \text{diag}[1/3, 1/3, 1/3]$ (i.e. $\psi(\theta, \varphi) = 1/4\pi$), and the FLDs in the SFCs are fractal and listed in Table 1. The RVEs of the SFCs are illustrated in Fig. 3, in which the corresponding FLDs of the RVEs are shown as well. It is noted that the sizes of the RVEs of the SFCs with the fractal FLDs are approximately 0.5 times the maximum fiber length by balancing RVE generation complexity, computational efficiency and FEH accuracy.

Here $\mathbf{a} = \text{diag}[1/3, 1/3, 1/3]$ leads to the macroscopically isotropic elastic properties of the SFCs.

Table 1 Fractal Parameters (i.e. the Minimum, Maximum and Average Aspect Ratios γ_1 , γ_m and $\bar{\gamma}$) for the FLD in the RVEs of the SFCs Consisting of the 2080 Aluminum Alloy and SiC Fibers.

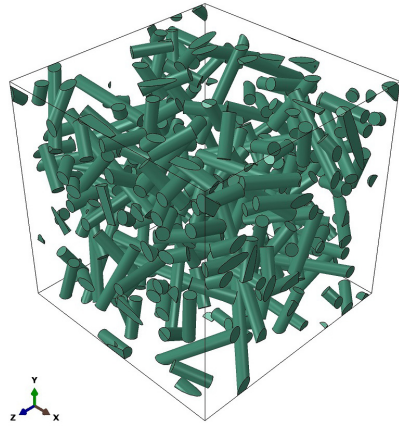
Fractal Parameter	Fiber Volume Fraction v_f		
	10.0%	20.0%	30.0%
γ_1	2.8	3.0	3.1
γ_m	40.0	50.0	60.0
$\bar{\gamma}$	5.0	5.0	5.0

The predicted elastic properties of the SFCs by the developed MSMFH method are plotted regarding the fiber volume fraction in Fig. 4, in which the predictions of the FEH method and the available experimental results³⁸ are presented as well. The relative errors between the results of the developed MSMFH method, the FEH method and the experimental tests are computed and less than 8.0%. The effectiveness of the developed MSMFH method and the proposed fractal FLD for the accurate predictions of the elastic properties of SFCs is thus validated.

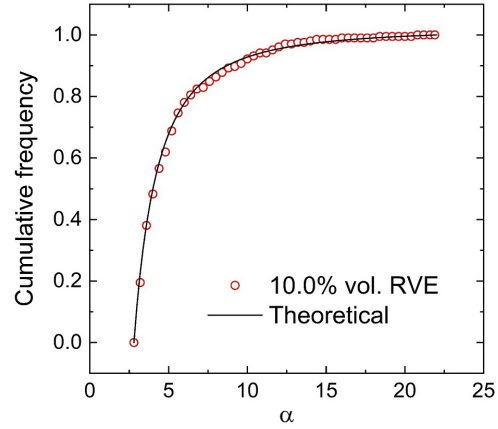
The second investigated SFCs are the same with the previous SFCs, except for the fiber orientation $\mathbf{a} = \text{diag}[1/2, 1/2, 0]$ (i.e. $\psi(\theta, \varphi) = 1/2\pi$) and the fiber volume fraction $v_f = 10.0\%$. The RVE of the SFCs and the corresponding FLD of the RVE are illustrated in Fig. 5. The estimations of the in-plane (i.e. the xoy plane) and out-plane elastic properties of the SFCs of the developed MSMFH method and the FEH method are compared in Table 2, which states that the differences between the predictions of these two methods are neglectable. The developed MSMFH method and the proposed fractal FLD are thus verified to accurately predict the elastic properties of SFCs.

The third type of SFCs are the short carbon fibers reinforced AZ91D magnesium alloy matrix SFCs.⁴⁰ The fiber volume fraction v_f is 10.0%, and the linear elastic properties of the matrix and fibers are $E_0 = 45.0$ GPa, $\mu_0 = 0.35$ and $E_1 = 230.0$ GPa, $\mu_1 = 0.25$. The second-order orientation vector of the fibers in the SFCs is $\mathbf{a} = \text{diag}[1/3, 1/3, 1/3]$ (i.e. $\psi(\theta, \varphi) = 1/4\pi$), and the FLD in the SFCs is fractal with $\gamma_1 = 8.4$, $\gamma_m = 120.0$ and $\bar{\gamma} = 15.0$. The RVE of the SFCs and the fractal FLD of the RVE are given in Fig. 6. Compared with the results of the FEH method and the available experimental tests,⁴⁰ the elastic properties of the SFCs predicted using the developed MSMFH method are listed in Table 3. It is found that the predictions of the developed MSMFH method agree well with the results of the FEH method and the experimental tests, and it thus indicates the developed MSMFH method and the proposed fractal FLD are capable of accurately predicting the elastic properties of SFCs.

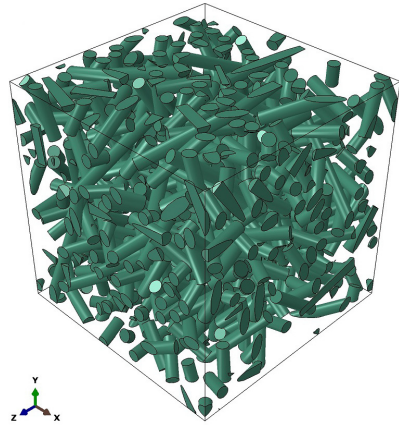
The additional SFCs consisting of the polypropylene matrix and the different volume fractions of glass fibers⁴¹ are studied. The elastic properties of the matrix and fibers are isotropic: $E_0 = 1.6$ GPa, $\mu_0 = 0.35$ and $E_1 = 75.0$ GPa, $\mu_1 = 0.25$. The



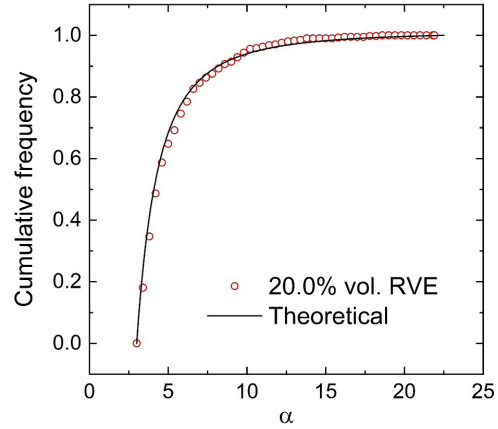
(a)



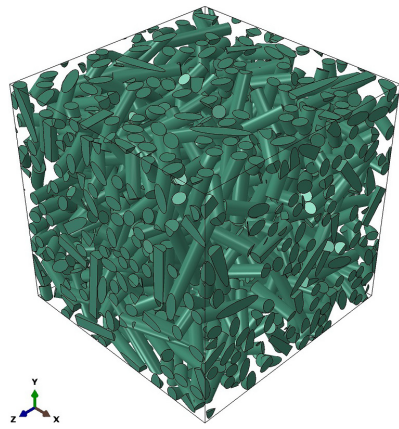
(b)



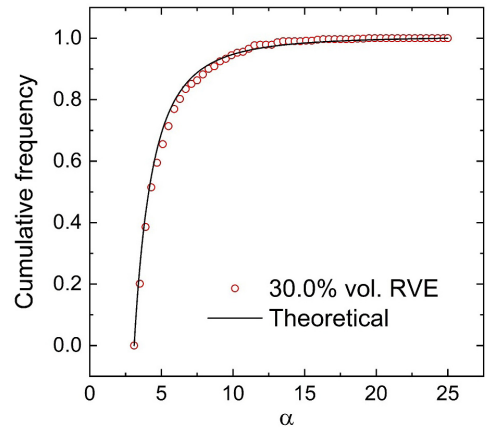
(c)



(d)



(e)



(f)

Fig. 3 RVEs of the SFCs consisting of the 2080 aluminum alloy and SiC fibers with $\mathbf{a} = \text{diag}[1/3, 1/3, 1/3]$ and the corresponding FLDs in these RVEs: (a)–(b) $v_f = 10.0\%$, (c)–(d) $v_f = 20.0\%$ and (e)–(f) $v_f = 30.0\%$.

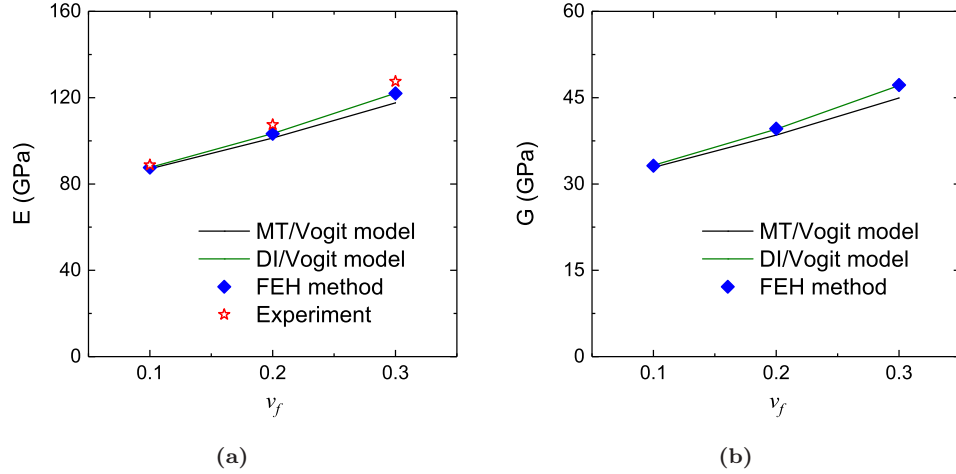


Fig. 4 Elastic properties of the SFCs consisting of the 2080 aluminum alloy and SiC fibers with $\mathbf{a} = \text{diag}[1/3, 1/3, 1/3]$ predicted using the developed MSMFH method and the FEH method and obtained from the experimental tests³⁸: (a) Elastic modulus E and (b) Shear modulus G . MT/Voigt and DI/Voigt denote that the MT and DI model are used to homogenize the SPGs in step (1) homogenization, respectively, and the Voigt model is used to homogenize all the SPGs and PGs in the sequential-step homogenization.

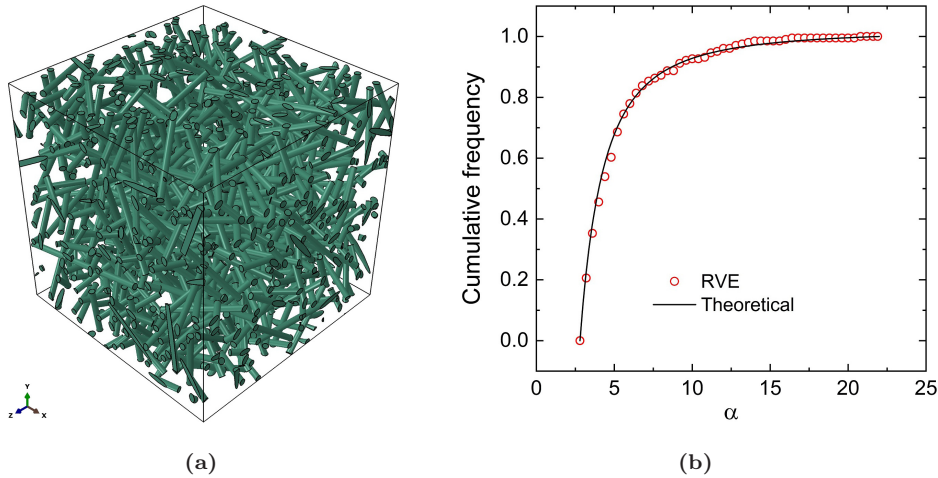


Fig. 5 RVE of the SiC fibers reinforced 2080 aluminum composites with $v_f = 10.0\%$ and $\mathbf{a} = \text{diag}[1/2, 1/2, 0]$ and the corresponding FLD of the RVE: (a) RVE and (b) FLD.

Table 2 Predicted In-Plane and Out-Plane Elastic Properties of the SiC Fibers Reinforced 2080 Aluminum Composites with $v_f = 10.0\%$ and $\mathbf{a} = \text{diag}[1/2, 1/2, 0]$ Using the Developed MSMFH Method and the FEH Method.

	Elastic Modulus (GPa)		Shear Modulus (GPa)	
	E_{11}	E_{33}	G_{12}	G_{13}
MT/Voigt model	88.86	85.38	33.74	32.05
DI/Voigt model	89.09	85.63	33.87	32.16
FEH method	89.21	86.53	33.89	32.48

fibers in the SFCs pertain to perfect planar random arrangements and the corresponding second-order orientation vector is thus $\mathbf{a} = \text{diag}[1/2, 1/2, 0]$ (i.e. $\psi(\theta, \varphi) = 1/2\pi$). The FLDs in the SFCs are assumed to be fractal and listed in Table 4 regarding the fiber volume fraction. The elastic properties of the SFCs are predicted by using the developed MSMFH method and then compared with the results of the FEH method and the experimental tests,^{41,42} as shown in Fig. 7. The maximum deviations of the predictions of the developed MSMFH method from the results of the FEH method and

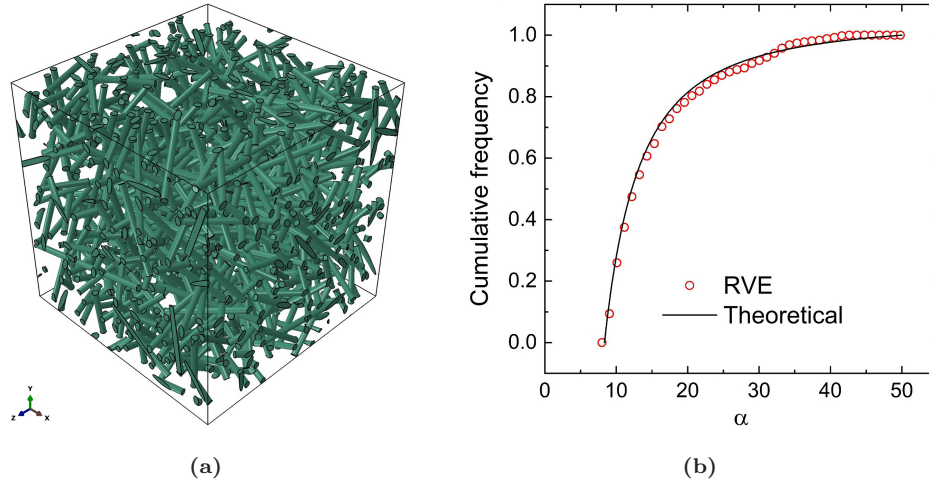


Fig. 6 RVE of short carbon fibers reinforced AZ91D magnesium alloy matrix SFCs with $\alpha = \text{diag}[1/3, 1/3, 1/3]$ and the corresponding FLD of the RVE: (a) RVE and (b) FLD.

Table 3 Elastic and Shear Moduli of Short Carbon Fibers Reinforced AZ91D Magnesium Alloy Matrix SFCs Obtained Using the Developed MSMFH Method, the FEH Method and the Experimental Tests.

	Elastic Properties (GPa)			
	MT/Voigt Model	DI/Voigt Model	FEH Method	Experiment
Elastic modulus	53.42	53.55	53.08	50.45
Shear modulus	19.93	19.98	19.76	19.02

Table 4 Fractal Parameters (i.e. the Minimum, Maximum and Average Aspect Ratios γ_1 , γ_m and $\bar{\gamma}$) for the FLD in the RVEs of the SFCs Consisting of the Polypropylene Matrix and Glass Fibers.

Fractal Parameter	Fiber Volume Fraction v_f		
	10.33%	12.89%	18.72%
γ_1	130	132	137
γ_m	2000	1600	1850
$\bar{\gamma}$	231	231	231

the experimental tests are computed as 8.78% and 6.46%, respectively, which indicates the validation of the developed MSMFH method and the proposed fractal FLD to accurately predict the elastic properties of SFCs.

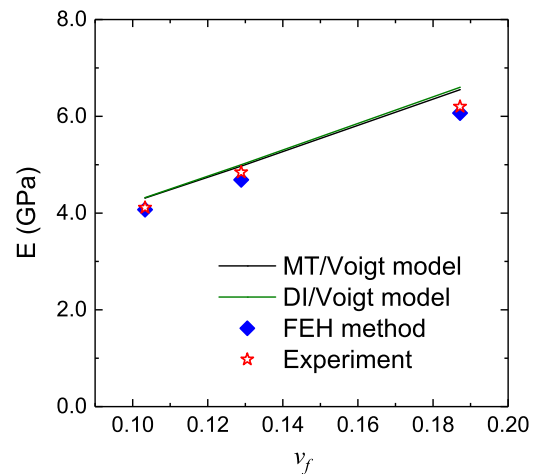


Fig. 7 Elastic moduli of the SFCs consisting of the polypropylene matrix and the glass fibers with $\alpha = \text{diag}[1/2, 1/2, 0]$ predicted using the developed MSMFH method and the FEH method and obtained from the experimental tests.^{41,42}

7. CONCLUSIONS

Resulting from different FODs and FLDs, the micro-structures of SFCs are very complicated. To accurately determine the mechanical properties of SFCs, the FOD and FLD are supposed to be fully considered. Based on the fractal theory, a fractal FLD function is proposed to characterize the fiber lengths of SFCs, and the MSMFH method is developed to accurately and efficiently predict the mechanical properties of SFCs with the fractal FLD.

In the developed MSMFH method, SFCs are first decomposed into a set of virtual PGs according to the FOD, followed the further division of the PGs into a large number of virtual SPGs according to the FLD. The MT or DI model is adopted for homogenizing the mechanical properties of each SPG in the step (1) homogenization, and the Voigt model is used for homogenizing the mechanical properties of all the SPGs and the PGs in the steps (2) and (3) homogenization. The fiber length and orientation averaging algorithms are introduced in the MSMFH method to take into account various FODs and FLDs of SFCs.

Regarding the different FODs, the mechanical properties of SFCs are predicted using the developed MSMFH method and the proposed fractal FLD, and compared with those of the FEH method and the available experimental tests. The results indicate the validation of the developed MSMFH method and the proposed fractal FLD to accurately and efficiently predict the mechanical properties of SFCs.


ACKNOWLEDGMENTS

This work is financially supported by the Guangdong Basic and Applied Basic Research Foundation (No. 2021A1515110034), the Natural Science Basic Research Plan in Shaanxi Province of China (No. 2022JQ-029), the Fundamental Research Funds for the Central Universities (No. 31020210502001) and the National Natural Science Foundation of China (Nos. 51472203 and 51772245), and the authors thank these supports.

ORCID

Wenlong Tian  <https://orcid.org/0000-0002-3155-4933>

Lu Zhu  <https://orcid.org/0009-0003-4454-1781>

Xujiang Chao  <https://orcid.org/0000-0002-0841-1790>

Lehua Qi  <https://orcid.org/0000-0001-5657-3658>

M. W. Fu  <https://orcid.org/0000-0002-0409-9701>

REFERENCES

1. W. Tian, L. Qi, J. Zhou, J. Liang and Y. Ma, Representative volume element for composites reinforced by spatially randomly distributed discontinuous fibers and its applications, *Compos. Struct.* **131** (2015) 366–373.
2. C. Kahl, M. Feldmann, P. Sälzer and H.-P. Heim, Advanced short fiber composites with hybrid reinforcement and selective fiber-matrix-adhesion based on polypropylene — characterization of mechanical properties and fiber orientation using high-resolution x-ray tomography, *Compos. Part A: Appl. Sci. Manuf.* **111** (2018) 54–61.
3. C. Mo, Y. Jiang and J. R. Raney, Microstructural evolution and failure in short fiber soft composites: Experiments and modeling, *J. Mech. Phys. Solids* **141** (2020) 103973.
4. S. Tamboura, M. Laribi, J. Fitoussi, M. Shirinbayan, R. T. Bi, A. Tcharkhtchi and H. B. Dali, Damage and fatigue life prediction of short fiber reinforced composites submitted to variable temperature loading: Application to sheet molding compound composites, *Int. J. Fatigue* **138** (2020) 105676.
5. P. A. Hessman, T. Riedel, F. Welschinger, K. Hornberger and T. Böhlke, Microstructural analysis of short glass fiber reinforced thermoplastics based on x-ray micro-computed tomography, *Compos. Sci. Technol.* **183** (2019) 107752.
6. R. Karamov, L. M. Martulli, M. Kerschbaum, I. Sergeichev, Y. Swolfs and S. V. Lomov, Micro-CT based structure tensor analysis of fibre orientation in random fibre composites versus high-fidelity fibre identification methods, *Compos. Struct.* **235** (2020) 111818.
7. S. Mortazavian and A. Fatemi, Effects of fiber orientation and anisotropy on tensile strength and elastic modulus of short fiber reinforced polymer composites, *Compos. Part B: Eng.* **72** (2015) 116–129.
8. Z. Rasheva, G. Zhang and T. Burkhart, A correlation between the tribological and mechanical properties of short carbon fibers reinforced peek materials with different fiber orientations, *Tribol. Int.* **43**(8) (2010) 1430–1437.
9. D. Notta-Cuvier, F. Lauro and B. Bennani, Modelling of progressive fibre/matrix debonding in short-fibre reinforced composites up to failure, *Int. J. Solids Struct.* **66** (2015) 140–150.
10. Y.-G. Hu, Y. Ma, C. Hu, X. Lu and S. Gu, Analysis of stress transfer in short fiber-reinforced composites with a partial damage interface by a shear-lag model, *Mech. Mater.* **160** (2021) 103966.
11. S.-Y. Fu and B. Lauke, Effects of fiber length and fiber orientation distributions on the tensile strength of short-fiber-reinforced polymers, *Compos. Sci. Technol.* **56**(10) (1996) 1179–1190.

12. F. Lionetto, F. Montagna, D. Natali, F. De Pascalis, M. Nacucchi, F. Caretto and A. Maffezzoli, Correlation between elastic properties and morphology in short fiber composites by x-ray computed micro-tomography, *Compos. Part A: Appl. Sci. Manuf.* **140** (2021) 106169.
13. W. Tian, X. Chao, M. Fu, L. Qi and L. Ju, New numerical algorithm for the periodic boundary condition for predicting the coefficients of thermal expansion of composites, *Mech. Mater.* **154** (2021) 103737.
14. Y. J. Cho, W. J. Lee and Y. H. Park, Effect of boundary conditions on plasticity and creep behavior analysis of particle reinforced composites by representative volume element approach, *Comput. Mater. Sci.* **100** (2015) 67–75.
15. N. Mentges, B. Dashtbozorg and S. Mirkhalaf, A micromechanics-based artificial neural networks model for elastic properties of short fiber composites, *Compos. Part B: Eng.* **213** (2021) 108736.
16. K. Babu, P. Mohite and C. Upadhyay, Development of an RVE and its stiffness predictions based on mathematical homogenization theory for short fibre composites, *Int. J. Solids Struct.* **130–131** (2018) 80–104.
17. H. Liu, D. Zeng, Y. Li and L. Jiang, Development of RVE-embedded solid elements model for predicting effective elastic constants of discontinuous fiber reinforced composites, *Mech. Mater.* **93** (2016) 109–123.
18. S. Yu, J. Y. Hwang and S. H. Hong, 3d microstructural characterization and mechanical properties determination of short basalt fiber-reinforced polyamide 6, 6 composites, *Compos. Part B: Eng.* **187** (2020) 107839.
19. X. Chao, W. Tian, F. Xu and D. Shou, A fractal model of effective mechanical properties of porous composites, *Compos. Sci. Technol.* **213** (2021) 108957.
20. B. Yu and J. Li, Some fractal characters of porous media, *Fractals* **09**(3) (2001) 365–372.
21. R. Hill, Elastic properties of reinforced solids: Some theoretical principles, *J. Mech. Phys. Solids* **11**(5) (1963) 357–372.
22. W. Voigt, Ueber die beziehung zwischen den beiden elasticitätsconstanten isotroper körper, *Ann. Phys.* **274**(12) (1889) 573–587.
23. A. Reuss, Berechnung der fließgrenze von mischkristallen auf grund der plastizitätsbedingung für einkristalle, *Z. Angew. Math. Mech.* **9**(1) (1929) 49–58.
24. T. Mori and K. Tanaka, Average stress in matrix and average elastic energy of materials with misfitting inclusions, *Acta Metall.* **21**(5) (1973) 571–574.
25. M. Hori and S. Nemat-Nasser, Double-inclusion model and overall moduli of multi-phase composites, *Mech. Mater.* **14**(3) (1993) 189–206.
26. J. D. Eshelby and R. E. Peierls, The determination of the elastic field of an ellipsoidal inclusion, and related problems, *Proc. R. Soc. London, Ser. A* **241**(1226) (1957) 376–396.
27. G. Lielens, P. Pirotte, A. Coumiot, F. Dupret and R. Keunings, Prediction of thermo-mechanical properties for compression moulded composites, *Compos. Part A: Appl. Sci. Manuf.* **29**(1) (1998) 63–70.
28. W. Tian, L. Qi, C. Su, J. Liang and J. Zhou, Numerical evaluation on mechanical properties of short-fiber-reinforced metal matrix composites: Two-step mean-field homogenization procedure, *Compos. Struct.* **139** (2016) 96–103.
29. O. Pierard, C. Friebel and I. Doghri, Mean-field homogenization of multi-phase thermo-elastic composites: A general framework and its validation, *Compos. Sci. Technol.* **64**(10) (2004) 1587–1603.
30. B. Yu, L. J. Lee and H. Cao, A fractal in-plane permeability model for fabrics, *Polym. Compos.* **23**(2) (2002) 201–221.
31. B. Jiang, C. Liu, C. Zhang, B. Wang and Z. Wang, The effect of non-symmetric distribution of fiber orientation and aspect ratio on elastic properties of composites, *Compos. Part B: Eng.* **38**(1) (2007) 24–34.
32. W. Tian, L. Qi and M. Fu, Multi-scale and multi-step modeling of thermal conductivities of 3d braided composites, *Int. J. Mech. Sci.* **228** (2022) 107466.
33. I. Doghri and L. Tinel, Micromechanics of inelastic composites with misaligned inclusions: Numerical treatment of orientation, *Comput. Methods Appl. Mech. Eng.* **195**(13) (2006) 1387–1406.
34. Q. Wu, C. Chen, N. Yoshikawa, J. Liang and N. Morita, Microscopic stresses of discontinuous fiber reinforced composites under thermal and mechanical loadings — finite element simulations and statistical analyses, *Comput. Mater. Sci.* **200** (2021) 110777.
35. K. Shingare and S. Naskar, Probing the prediction of effective properties for composite materials, *Eur. J. Mech. A Solids* **87** (2021) 104228.
36. W. Tian, X. Chao, M. Fu and L. Qi, An advanced method for efficiently generating composite RVEs with specified particle orientation, *Compos. Sci. Technol.* **205** (2021) 108647.
37. M. Herráez, J. Segurado, C. González and C. Lopes, A microstructures generation tool for virtual ply property screening of hybrid composites with high volume fractions of non-circular fibers — viper, *Compos. Part A: Appl. Sci. Manuf.* **129** (2020) 105691.

38. W. Tian, L. Qi, X. Chao, J. Liang and M. Fu, Periodic boundary condition and its numerical implementation algorithm for the evaluation of effective mechanical properties of the composites with complicated micro-structures, *Compos. Part B: Eng.* **162** (2019) 1–10.
39. Y. Hua and L. Gu, Prediction of the thermomechanical behavior of particle-reinforced metal matrix composites, *Compos. Part B: Eng.* **45**(1) (2013) 1464–1470.
40. L. Qi, W. Tian and J. Zhou, Numerical evaluation of effective elastic properties of composites reinforced by spatially randomly distributed short fibers with certain aspect ratio, *Compos. Struct.* **131** (2015) 843–851.
41. Z. Lu, Z. Yuan and Q. Liu, 3d numerical simulation for the elastic properties of random fiber composites with a wide range of fiber aspect ratios, *Comput. Mater. Sci.* **90** (2014) 123–129.
42. J. Thomason and M. Vlug, Influence of fibre length and concentration on the properties of glass fibre-reinforced polypropylene: 1. Tensile and flexural modulus, *Compos. Part A: Appl. Sci. Manuf.* **27**(6) (1996) 477–484.